URSI GASS 2020, Rome, Italy; 29 Aug. - 5 Sep. 2020

Simultaneous Observation of Electromagnetic Ion Cyclotron and Magnetosonic Waves

S. Teng[(1),(2)], X. Tao[(1),(2)], Y. Wu[(1),(2)], W. Li[(3)] and Q. Ma[(4),(3)]

(1)CAS Key Laboratory of Geospace Environment, Department of Geophysics and Planetary Sciences, University of Science and Technology of China, Hefei, China
(2)CAS Center for Excellence in Comparative Planetology, China,
(3)Center for Space Physics, Boston University, Boston, MA, USA,
(4)Department of Atmospheric and Oceanic Sciences, University of California, Los Angeles, Los Angeles, CA, USA

Abstract

We report the simultaneous observation of Electromagnetic Ion Cyclotron (EMIC) waves and Magnetosonic (MS) waves, which can be categorized into two mechanisms. The first one is that MS waves potentially cause the resonant heating of cold protons and the temperature anisotropy of cold protons (10–100 eV) likely provides free energy for the excitation of high frequency EMIC waves. This type of high frequency EMIC waves has a very narrow frequency bandwidth, closely following and approaching the proton gyrofrequency. The second one is the simultaneous generation of EMIC waves and MS waves. The particle-in-cell simulations have demonstrated that a ring-like proton velocity distribution and which is sufficiently anisotropic can excite alfven-cyclotron and ion bernstein instability. Here we present the observation to show that the anisotropic ring-like distribution could be the source of EMIC and MS waves. These observations provide new insights into understanding the generation of EMIC and MS waves and the energy transfer process between MS waves and EMIC waves.

1 Introduction

Electromagnetic ion cyclotron (EMIC) waves and magnetosonic (MS) waves are intense emissions, naturally occurring in the Earth's magnetosphere. A typical source of EMIC waves is the anisotropic distribution of energetic ions (1–100 keV), preferentially near the equatorial region (Chen et al. 2009; Cornwall, 1965). MS waves are generally thought to be driven by energetic protons at energies of tens of keV with a ring−like distribution when the ring velocity is within a factor of 2 above or below the Alfvenic speed (Chen et al., 2010; Jordanova et al., 2012; Liu et al., 2011). Recent particle-in-cell (PIC) simulations (Min et al., 2016) have demonstrated that a ring-like proton velocity distribution with and which is sufficiently anisotropic can excite alfven-cyclotron and ion bernstein instability. However, there have been few reports on the simultaneous observation of EMIC and MS waves. Only Yuan et al. (2019) reported simultaneous trapping of EMIC and MS waves by background plasmas. In this work, we present the simultaneous observation of EMIC and MS waves. They can be divided into two categories based on their generation mechanisms. One proposes that MS waves could heat cold protons in the perpendicular direction and anisotropic proton distribution could provide free energy for the excitation of high frequency EMIC waves. Another one provides the evidence for the above PIC simulation result that EMIC and MS waves could be generated by anisotropic ring-like distribution.

2 Observation: Mechanism I

Figure 1 shows a typical event illustrating the first generation mechanism for the simultaneous observation of EMIC and MS waves.

EMIC and MS waves were observed in the morning sector (7.7–9.1 MLT) over the L−shells of 4.9–5.7 near the geomagnetic equator (−2.5°–0.6° MLAT) during a modest substorm activity. Figure 1b-c shows the presence of MS waves. Figure 1d shows the proton flux observed by HOPE and their pitch angle distributions at the energy of 98 eV and 210 eV are shown in Figures 1e and 1f. Figure 1g-h demonstrate the unusual high frequency EMIC waves. The

close correlation between MS waves, pancake distribution of cold proton implies the possible proton heating due to MS waves. High frequency EMIC waves is possibly generated by anisotropic distribution of cold proton.

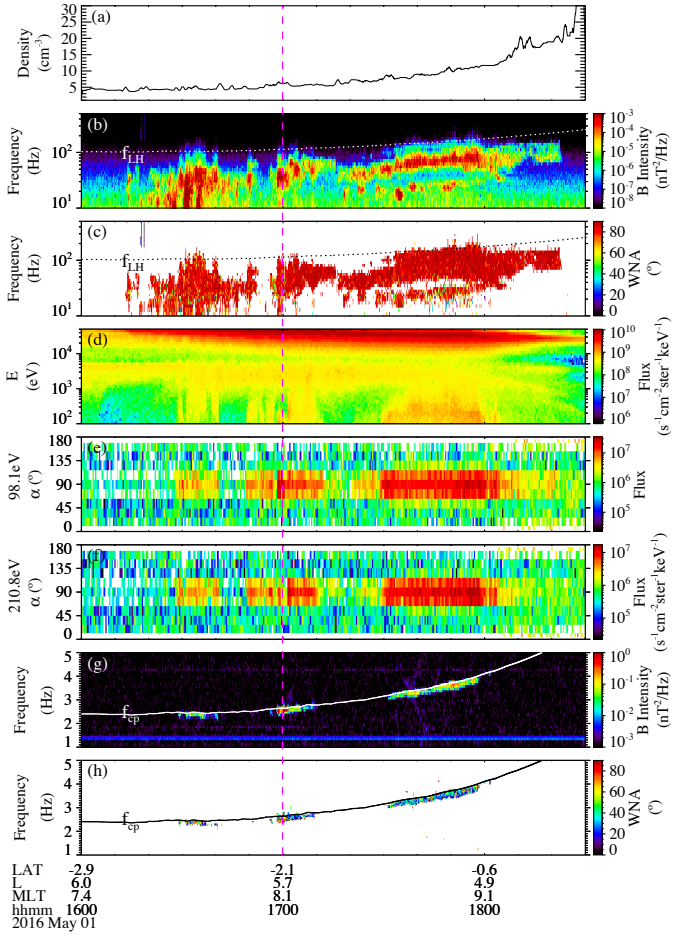

Figure 1. An overview of Van Allen Probe A observation on 1 May 2016. (a) The electron density profile (b) Magnetic power spectrogram (c) wave normal angle (WNA), shown in the frequency range from 10 to 500 Hz. In panels (b) and (c), the white or black dotted line represents lower hybrid resonance frequency (f_{LH}). (d) Energy spectrogram of spin-averaged proton flux. (e and f) Pitch angle distributions of proton fluxes at energies of ~98.1 and 210.8 eV. (g) Magnetic power spectrogram and (h) wave normal angle shown in the frequency range from 1 to 5 Hz. The solid lines (white or black) in panels (g) and (h) represent the local proton gyrofrequency (f_{cp}). The vertical magenta dashed line indicates the time used for the linear growth rate calculation.

3 Linear Growth Rate Calculation

The proton distribution from 1 eV to 50 keV measured by HOPE (Figure 1d) was used to evaluate the linear growth rate of high frequency EMIC waves based on the actual proton velocity distribution and plasma parameters. Figure 2a presents the parallel (red) and transverse (black) proton phase space densities (PSDs) and Figure 2b shows the 2-D proton PSD distribution in the energy range between 0 and 200 eV at the time indicated by the vertical magenta line in Figure 1. The cyclotron resonance energy of protons for the observed EMIC wave peak frequency of ~0.92 f_{cp} (black) and the typical H$^+$ band EMIC wave frequency ~0.45 f_{cp} (blue), which are shown as a function of pitch angle in Figure 2c. The resonance energy for high frequency EMIC waves is much lower, ranging from tens to hundreds of eV. Figure 2d shows the comparison of the calculated wave growth rate using the BO kinetic dispersion relation solver (blue) and the observed wave intensity (black) (Xie & Yong, 2016). The cold proton temperature anisotropy is mainly responsible for the excitation of high frequency EMIC waves.

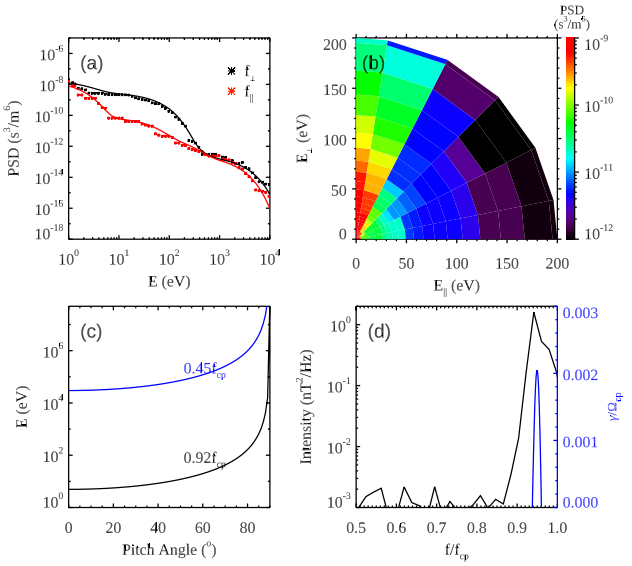

Figure 2. The proton distribution, proton resonance energy, and calculated EMIC wave growth rate at ~17 UT on 1 May 2016, marked by the vertical magenta line in Figure 1. (a) Parallel (red) and transverse (black) proton phase space density (PSD) measured by HOPE (dotted line) and the corresponding multicomponent fits (solid line). (b) The proton PSD distributions in the parallel and perpendicular energy space. (c) The calculated resonance energy as a function of pitch angle at the observed wave frequency ~0.92 f_{cp} (black) and the typical H$^+$ band EMIC wave frequency ~0.45 f_{cp} (blue). (d) The comparison between the observed EMIC wave intensity (black) and the calculated linear wave growth rate (blue) using the hot plasma dispersion relation.

4 Observation: Mechanism II

Figure 3 shows another case of the simultaneous observation of MS and EMIC waves possibly generated by anisotropic

proton ring distribution. Figure 3a indicates the waves were observed outside the plasmapause. Figure 3b-c, g-h show MS wave characteristics. Figure 3d-e, i-j are for EMIC wave characteristics. They are potentially generated locally.

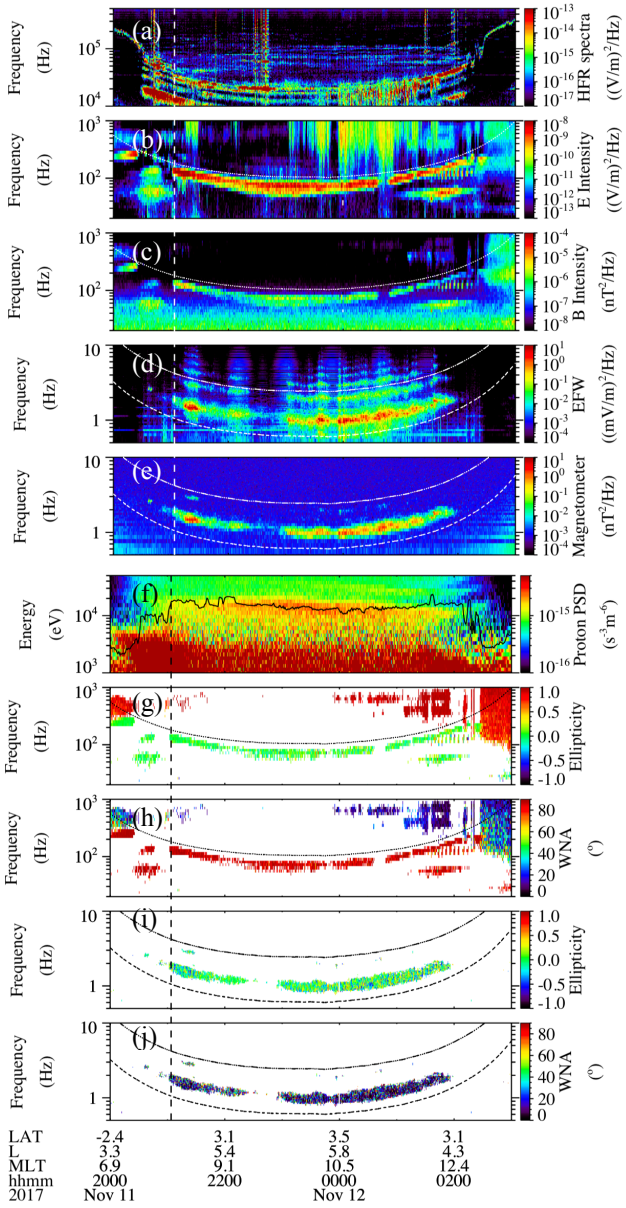

Figure 3. An overview of Van Allen Probe B observation on 11 Nov 2017. (a) HFR spectra (b) Electric field and (c) magnetic field intensity shown in the frequency range from 1 to 1000 Hz. (d) Electric field and (e) magnetic field intensity shown in the frequency range from 0.5 to 10 Hz. (f) Energy spectrogram of spin−averaged proton phase space density with the black line indicating the Alven energy. (g)(i) Ellipticity and (h)(j) wave normal angle. In panels (b) (c) (g) and (h), the white or black solid line represents lower hybrid resonance frequency (f_{LH}). In panels (d) (e) (i) and (j), the white or black solid and solid-dot lines represent proton(f_{cp}) and helium gyrofrequency (f_{cHe}). The vertical dashed line indicates the time used for the linear growth rate calculation.

5 Linear Growth Rate Calculation

Figure 4 shows the comparison of the observed and fitted proton phase space density. The fitted result is a combination of several bi-maxwellian distribution and a partial-shell distribution.

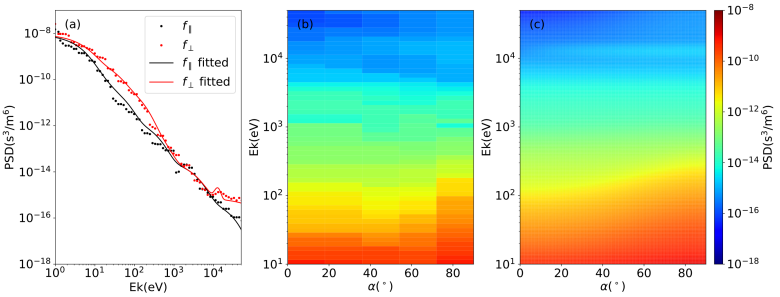

Figure 4. (a) Parallel (black) and transverse (red) proton phase space density (PSD) measured by HOPE (dotted line) and the corresponding multicomponent fits (solid line). 2D (b) observed and (c) fitted proton distribution.

The linear growth rate was calculated using the fitted proton phase space density and compared with the observed wave intensity, shown in Figure 5. As can be seen, the calculated results agree well with the EMIC and MS wave intensity.

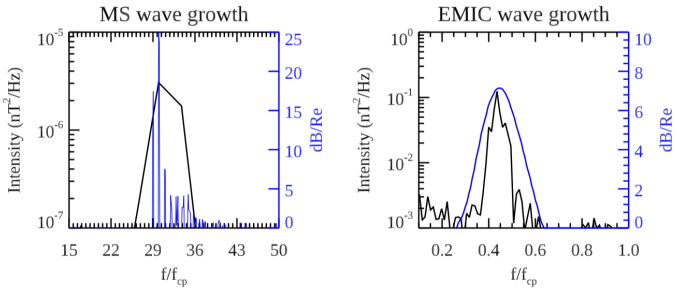

Figure 5. The comparison between the observed MS (left) and EMIC (right) wave intensity (black) and the calculated linear wave growth rate (blue).

6 Conclusion

In this work, we show the simultaneous observation of EMIC and MS waves using Van Allen Probes data. Based on the generation mechanism, these observations can be categorized into two groups. One is the energy coupling between MS and EMIC waves, which is MS waves heat the cold protons in the perpendicular direction and anisotropic cold protons provide free energy for the excitation of high frequency EMIC waves. This mechanism remains to be tested in the future PIC simulation. Another one is the simultaneous generation of EMIC and MS waves by anisotropic proton, which has already been demonstrated in

previous PIC simulations.

7 Acknowledgements

This work was supported by NSFC grants 41631071, 41674174, and 41474142. WL and QM would like to acknowledge the NSF grant AGS−1723588 and the Alfred P. Sloan Research Fellowship FG−2018− 10936.

References

[1] Chen, L., Thorne, R. M., & Horne, R. B. (2009). "Simulation of EMIC wave excitation in a model magnetosphere including structured high− density plumes," *Journal of Geophysical Research*, **114**, A07221. https://doi.org/10.1029/2009JA014204

[2] Chen, L., Thorne, R. M., Jordanova, V. K., & Horne, R. B. (2010). "Global simulation of magnetosonic wave instability in the storm time magnetosphere," *Journal of Geophysical Research*, 115, A11222. https://doi.org/ 10.1029/2010JA015707

[3] Cornwall, J. M. (1965). "Cyclotron instabilities and electromagnetic emission in the ultra low frequency and very low frequency ranges," *Journal of Geophysical Research*, **70**, 61–69. https://doi.org/10.1029/ JZ070i001p00061

[4] Jordanova, V., Welling, D., Zaharia, S., Chen, L., & Thorne, R. (2012). "Modeling ring current ion and electron dynamics and plasma instabilities during a high−speed stream driven storm," J*ournal of Geophysical Research*, **117**, A00L08. https://doi.org/ 10.1029/ 2011JA017433

[5] Liu, K., Gary, S. P., & Winske, D. (2011). "Excitation of magnetosonic waves in the terrestrial magnetosphere: Particle−in−cell simulations," *Journal of Geophysical Research*, **116**, A07212. https://doi.org/ 10.1029/2010JA016372

[6] Min, K., K. Liu, and S. Peter Gary (2016), "Scalings of Alfvén-cyclotron and ion Bernstein instabilities on temperature anisotropy of a ring-like velocity distribution in the inner magnetosphere," *J. Geophys. Res. Space Physics*, **121**, 2185–2193, doi:10.1002/2015JA022134.

[7] Teng, S., Li, W., Tao, X., Ma, Q., Wu, Y., Capannolo, L., et al. (2019). "Generation and characteristics of unusual high frequency EMIC waves," *Geophysical Research Letters*, **46**. https://doi.org/ 10.1029/2019GL085220

[8] Xie, H., & Yong, X. (2016). PDRK: A general kinetic dispersion relation solver for magnetized plasma. *Plasma Science and Technology*, **18(2)**, 97–107. https://doi.org/ 10.1088/1009−0630/18/2/01

[9] Yuan, Z., Yu, X., Ouyang, Z., Yao, F., Huang, S., & Funsten, H. O. (2019). "Simultaneous trapping of electromagnetic ion cyclotron and magnetosonic waves by background plasmas," *Journal of Geophysical Research: Space Physics*, **124**, 1635–1643. https:// doi.org/10.1029/ 2018JA026149